Electronic structure and weak electron-phonon coupling in TaB_2

H. Rosner* and W. E. Pickett
Department of Physics, University of California, Davis, California 95616

S.-L. Drechsler, A. Handstein, G. Behr, G. Fuchs, K. Nenkov, K.-H. Müller, and H. Eschrig
Institut für Festkörper- und Werkstofforschung Dresden e.V., Postfach 270116, D-01171 Dresden, Germany
(Received 1 June 2001; published 21 September 2001)

We present electronic structure calculations together with resistivity, susceptibility, and specific heat measurements for TaB_2 to search for the recently contradictorily reported superconductivity and to study related normal-state properties. We ascribe the absence of superconductivity down to 1.5 K for our TaB_2 samples to the generally weak electron-phonon coupling derived from comparison of the calculated and measured specific heat constants. For the E_{2g} and the B_{1g} Γ-point phonons, we derive from the calculated deformation potentials very small electron-phonon couplings for these modes, as opposed to the strong coupling of the E_{2g} mode in MgB_2, probably responsible for its high T_c. In comparison to MgB_2, we discuss the origin of the quite different features in the density of states and of the Fermi surfaces. The differences are mainly due to the strong hybridization between Ta $5d$ and B $2p$ states outside the hexagonal basis plane.

DOI: 10.1103/PhysRevB.64.144516 PACS number(s): 74.25.Jb, 74.25.Bt, 74.25.Fy, 71.20.−b

I. INTRODUCTION

The recent discovery of superconductivity in MgB_2 (Ref. 1) has initiated an immediate broad research activity due to the surprisingly high transition temperature $T_c \sim 40$ K in a seemingly ordinary s-p metal. Investigation of related s-p diborides MB_2 (M=Li, Be, Al) (Refs. 2–4) and a series of isostructural transition metal diborides (M=Sc, Ti, Zr, Hf, V, Ta, Cr, Mo, Nb) (Refs. 5–7) has shown that only few of them seem to be superconducting, and then only at very low temperatures. Since the understanding of the pairing mechanism in MgB_2 is still in its early stages, a study of the isomorphic compounds with low transition temperatures or with the absence of superconductivity, respectively, could be helpful in clarifying the expected very substantial electronic differences.

Contradictory reports about superconductivity in TaB_2 have appeared; one found superconductivity at $T_c \sim 9.5$ K,[8,9] while another found no superconductivity down to 4.4 K.[10] TaB_2 is isovalent with NbB_2, where the occurrence of superconductivity, or at least the value of T_c, is likewise uncertain. NbB_2 was reported to be superconducting at 3.87 K,[6] superconducting only at 0.62 K,[7] and not superconducting above 0.37 K.[10] Clearly there is sample dependence for both TaB_2 and NbB_2, and no doubt for many other diborides as well.

In an attempt to begin to settle some of these discrepancies, we address TaB_2 specifically in this paper with a joint theoretical (Secs. II A and III A) and experimental (Secs. II B and III B) investigation. In Sec. III we provide an analysis of its electronic structure and contrast it with that of MgB_2. We also present specific heat and susceptibility as well as resistivity data for two almost-single-phase samples. One of them exhibited a significant amount of boron vacancies.

II. METHODS

A. Band structure calculations

We calculated the electronic structure of TaB_2 in the hexagonal space group (SG) $P6_3/mmc$ (No. 191) with the lattice constants $a=3.082$ Å and $c=3.243$ Å.[8] The frozen phonon calculations for the E_{2g} and B_{1g} modes were done in the orthorhombic SG $Cmmm$ (No. 65) and in the trigonal SG $P\bar{3}m1$ (No. 164), respectively.

Our band structure calculations were performed using the full-potential nonorthogonal local-orbital minimum-basis (FPLO) scheme[11] within the local density approximation (LDA). In these scalar relativistic calculations we used the exchange and correlation potential of Perdew and Zunger.[12] Ta $5s$, $5p$, $6s$, $6p$, $5d$ states and B $2s$, $2p$, $3d$ were chosen as a minimum-basis set for the valence states. All lower-lying states were treated as core states. The inclusion of the relatively extended Ta $5s$, $5p$ semicore states as band states was done because of the considerable overlap of these states on nearest neighbors. This overlap would be otherwise neglected in our FPLO scheme. Accounting for this overlap is of importance especially for the calculations of phonon frequencies that we report. B $3d$ states were added to increase the quality of the basis set. The spatial extension of the basis orbitals, controlled by a confining potential[13] $(r/r_0)^4$, was optimized to minimize the total energy. The self-consistent potentials were carried out on a k mesh of 20 k points in each direction of the Brillouin zone, which corresponds to 481, 784, and 1221 in the irreducible part for $P6_3/mmc$, $P\bar{3}m1$, and $Cmmm$ SG's, respectively.

B. Sample preparation and measurements

Two different TaB_2 samples, one with near-stoichiometric and one with boron-deficient compositions, were prepared starting from the pure elements Ta (>99.9%) and B (>99.9%) by an arc melting furnace under purified argon atmosphere. To ensure a better homogeneity the samples were turned several times. The phase content was checked by x-ray diffraction (XRD) using Co $K\alpha$ radiation.

The samples contain the hexagonal AlB_2 phase mainly, 95% in sample No. 1 and 97% in sample No. 2. In both samples small amounts (<5%) of a second phase were found which are B for sample No. 1 and Ta_3B_4 for sample

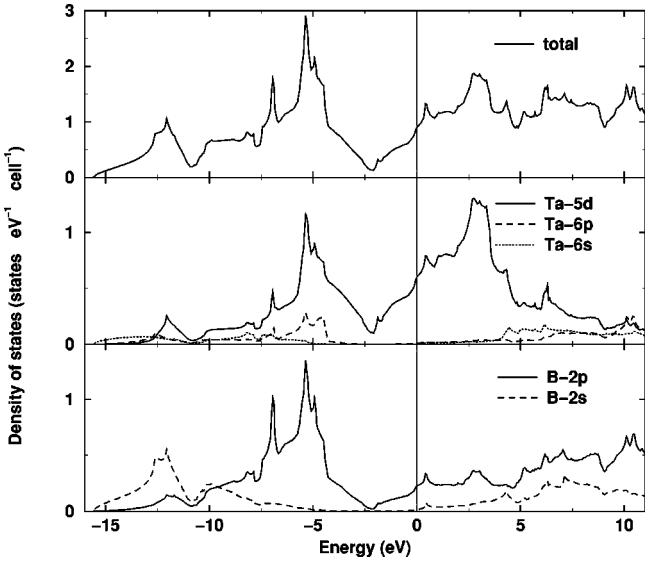

FIG. 1. Total DOS and partial DOS of TaB_2. The upper panel gives the total DOS, and the middle and the lower panels show the contribution of Ta and B, respectively. The Fermi level is at zero energy.

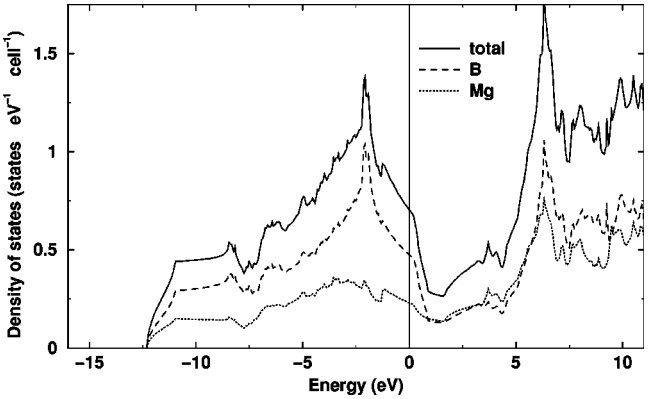

FIG. 2. Total DOS and partial DOS of MgB_2. The partial DOS are calculated by projection to the minimum orbital basis. The Fermi level is at zero energy.

No. 2. The compositions of the main phases measured by electron probe microanalysis in the wavelength dispersive x-ray analysis (WDX) modus showed a composition of about $TaB_{2.03}$ (sample No. 1) and compositions of $TaB_{1.29}$ (sample No. 2).

Furthermore, the XRD resulted in quite different lattice parameters for the two samples ranging from $a=3.098 \pm 0.002$ nm and $c=3.224\pm 0.003$ Å of the B-deficient sample to $a=3.067\pm 0.002$ Å and $c=3.286\pm 0.006$ Å of the B-rich sample.

The specific heat of both TaB_2 samples was measured in the temperature range between 2 and 16 K using a Quantum Design PPMS relaxation calorimeter. The addenda which were determined in a separate run were subtracted in order to obtain the specific heat data for TaB_2.

Magnetization measurements have been performed using a Quantum Design superconducting quantum interference device (SQUID) magnetometer in the temperature range down to 1.8 K. Resistivity measurements down to 1.5 K have been performed using the standard four-probe method.

III. RESULTS AND DISCUSSION

A. Theoretical results

In Fig. 1 we display the total as well as the atom-decomposed density of states (DOS) of TaB_2. The B $2p$ and Ta $5d$ states share almost equally in the occupied valence bands in the region -10 to -2 eV (the Fermi level $E=\varepsilon_F$ is taken as the zero of energy). Our DOS is in agreement with that of Singh,[14] which we became aware of right after the completion of our study.

A striking difference in comparison to MgB_2 is the dominating contribution of Ta $5d$ states to the DOS at the Fermi level, which contribute about 70% of the total DOS; in MgB_2 the DOS at the Fermi level is dominated by B $2p$ states (see Fig. 2 for a comparison[15]). Although a rigid band picture is very limited in this case, a valence analysis shows that due to the three additional valence electrons of Ta with respect to Mg, the Fermi level has shifted from the bonding B states below the hybridization gap in MgB_2 to the antibonding states above this gap in TaB_2 . From the very similar shape of the partial B and Ta DOS, a strong hybridization between B $2p$ and Ta $5d$ states is obvious, discussed below in more detail. The calculated value of the density of states at the Fermi level $N(\varepsilon_F)$ is slightly higher for TaB_2 $[N(\varepsilon_F)=0.91$ states/(eV$\times$cell)] than for MgB_2 $[N(\varepsilon_F)=0.71$ states/eV$\times$cell], in agreement with Refs. 16 and 17. This corresponds to a bare specific heat coefficient $\gamma_0=2.14$ mJ/(mol K^2) for TaB_2. Figure 3 shows the band structure of TaB_2 along the symmetry lines of the hexagonal cell. As already mentioned above, the bonding B σ states, which lie in the region -10 eV to -2 eV and are highlighted in the middle panel, are completely filled. These states, which are unoccupied along the Γ-A direction in MgB_2 (compare to Figs. 1 of Refs. 16 and 17), lie now between -5 eV and -2 eV for this symmetry line and show almost 3 eV dispersion compared to 0.6 eV in MgB_2. The two-dimensional character of these states in MgB_2 is obviously destroyed in TaB_2. Furthermore, we find around the A-L-H plane of the k space a strong hybridization of those B σ states with the Ta $5d_{xz}$ and $5d_{yz}$ states, indicated in the lower panel of Fig. 3. Once more we like to emphasize the difference to MgB_2 , where these states are of nearly pure B σ character. The corresponding Fermi surface (FS) of TaB_2 is shown in Fig. 4. For convenience of comparison with MgB_2 (compare to Fig. 3 in Ref. 17), we have chosen the A point as the center of the hexagonal prism. All three sheets of the FS of TaB_2 are electronlike. Because of the strong dispersion of the antibonding Bσ–Ta $5d_{xz,yz}$ states, they build closed FS's around the A point (see middle and lower panels of Fig. 4), where the holelike quasi two-dimensional tubes are found in MgB_2 . The large FS in the upper panel of Fig. 4 is due to Ta $5d$ states; the contribution of B states to this sheet is almost negligible.

To account for the experimental uncertainty in the lattice constants for different samples,[18] we also investigated the

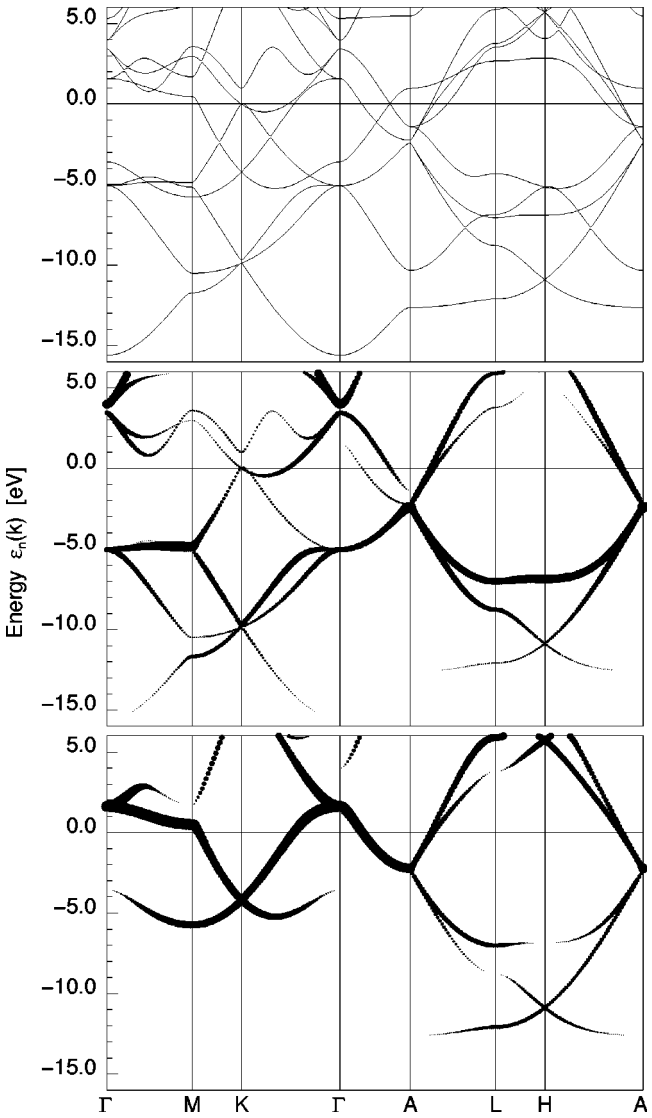

FIG. 3. Band structure and band characters of TaB_2. The middle and the lower panels show the band characters of the B $2p_{x,y}$ orbitals and the Ta $5d_{xz,yz}$ orbitals, respectively. The linewidth is scaled with the orbital weights of the corresponding orbitals.

influence of different lattice constants for the experimentally reported range on the electronic structure. The changes for the relevant features in the band structure are negligible, the DOS is basically unchanged, and $N(\varepsilon_F)$ varies by less than 2%.

For a rough estimate of the electron-phonon coupling in TaB_2 , we calculated the phonon frequencies and the deformation potential of the E_{2g} (in-plane displacement of the borons) and the B_{1g} (borons displaced along z in different directions) zone-center phonon modes. Their frequencies are 98 meV and 85 meV, respectively. For the corresponding frequencies in MgB_2 Kortus *et al.*[17] reported 58 meV and 86 meV, respectively. For AlB_2, 118 meV and 60 meV, respectively, were calculated.[19] Already from the strong hardening of the calculated E_{2g} frequency compared with MgB_2 one can conclude a strongly reduced electron-phonon coupling of this mode.

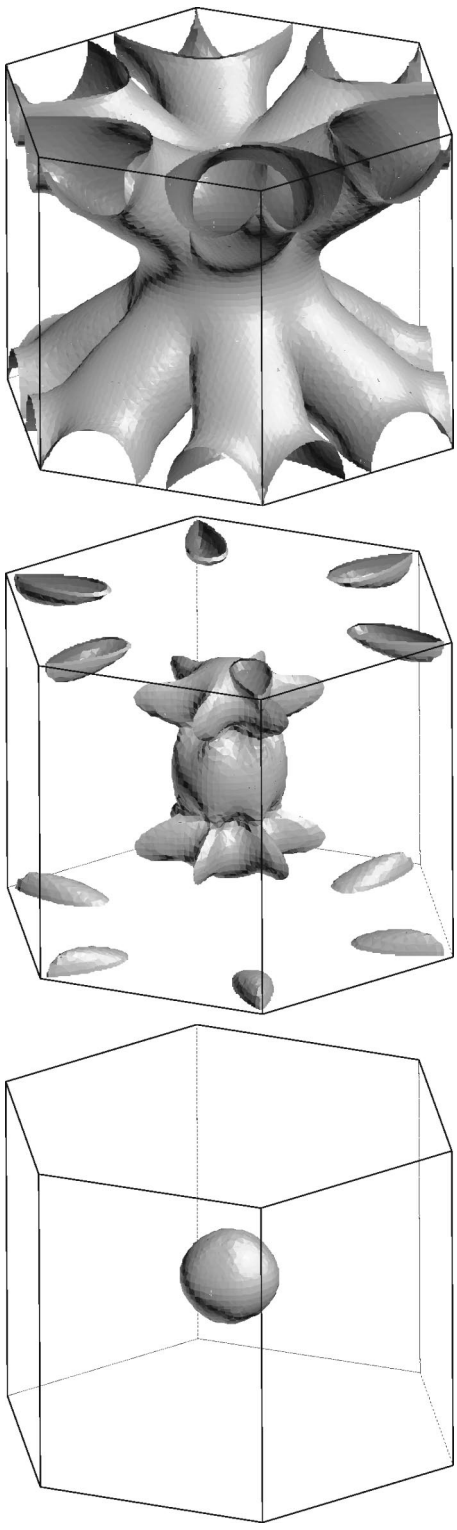

FIG. 4. The three different sheets of the Fermi surface of TaB_2, all sheets are electronlike. The *A* point corresponds to the center of the hexagonal prism; the Γ point is the midpoint of the lower and upper hexagon.

Figure 5 shows the calculated band structure for the frozen E_{2g} phonon mode of TaB_2 with a B displacement of $\Delta u_B = 0.018$ Å. The B bond stretching mode splits the antibonding B σ–Ta $5d_{xz,yz}$ bands along the Γ-*A* line. For an

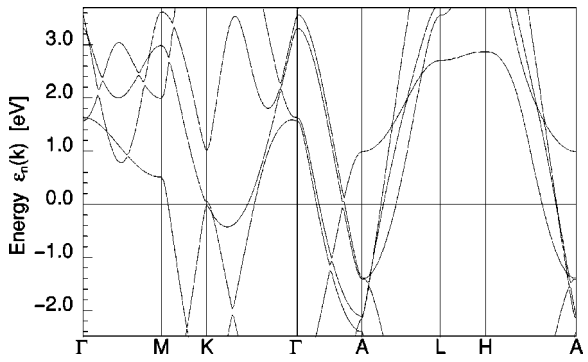

FIG. 5. Band structure for frozen E_{2g} mode, plotted along the same lines as in Fig. 3 to facilitate comparison. The two-fold degenerate bands in Fig. 3, crossing the Fermi level along the Γ-*A* direction, are split due to the symmetry-reducing phonon mode.

averaged split $\Delta\varepsilon_k/\Delta u_B \sim 9$ eV/Å we find a deformation potential $D_{E_{2g}} \sim 4.5$ eV/Å, about 3 times smaller than $D_{E_{2g}}$ in MgB_2.[16] Calculating larger elongations up to the actual rms we found a nearly linear dependence of the deformation potential $D_{E_{2g}}$ on the elongation Δu.

Following Ref. 16, we can estimate the coupling from this mode alone using Eq. (2.34) of Kahn and Allen[20] for the electron-phonon matrix element in terms of $D_{E_{2g}}$. With $N_{E_{2g}}(\varepsilon_F)=0.28$, resulting from a summation of the calculated orbital projected DOS for the orbitals mainly involved in the deformed band, we find

$$\lambda_{E_{2g}} = N_{E_{2g}}(\varepsilon_F)\left[\frac{\hbar}{2M_B\omega^2}\right]\left|\sum_{j=1,2}\hat{\varepsilon}_j D_j\right|^2 \sim 0.055. \qquad (1)$$

The sum on *j* runs over the two B atoms of the E_{2g} mode; for M_B, we used the isotope averaged mass of B. Due to the high frequency ω and the smaller deformation potential $D_{E_{2g}}$, we get a coupling smaller by a factor of about 20 compared to MgB_2 .

From a corresponding calculation of the coupling constant for the B_{1g} mode, reported[19] to be softened in AlB_2 (ω =60 meV), we find an even slightly smaller contribution compared with the already weak-coupled E_{2g} phonon.

Assuming similar coupling to the acoustic phonons as reported[19] for MgB_2 or AlB_2 and comparable contributions of other modes, the total el-ph coupling constant might be no more than $\lambda \sim 0.2$.

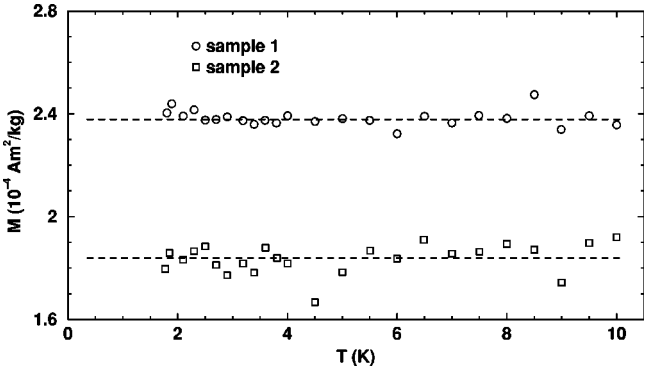

FIG. 7. Temperature-dependent magnetization *M* of two TaB_2 samples in the temperature range 1.8 K$<T<$10 K at an applied magnetic field of $H=10$ Oe.

B. Experimental results

The results of the specific heat measurements are shown in Fig. 6. Since no superconductivity was observed at least in the temperature range down to 1.8 K from magnetization measurements (see Fig. 7) and down to 1.5 K from resistance measurements (see Fig. 8), the results of the specific heat measurements are shown in the c_p/T vs T^2 plot. Thus, assuming standard normal metal behavior, the Sommerfeld coefficient γ was determined using the relation

$$c_p/T = \gamma + \frac{12}{5}R\pi^4\Theta_0^{-3}T^2, \qquad (2)$$

with *R* being the ideal gas constant and Θ_0 the initial Debye temperature.

The investigated TaB_2 samples show distinct anomalies at temperatures around 4 K which are, however, not due to

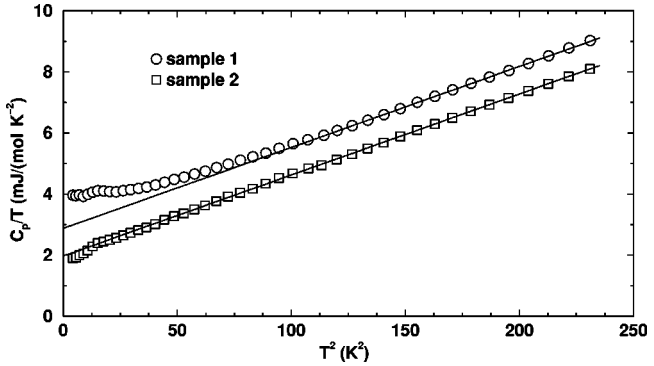

FIG. 6. Specific heat $c_p(T)/T$ vs T^2 of two TaB_2 samples at zero magnetic field. The lines correspond to linear regression fits of the experimental data for temperatures $T>8$ K (sample 1) and $T>4$ K (sample 2), respectively.

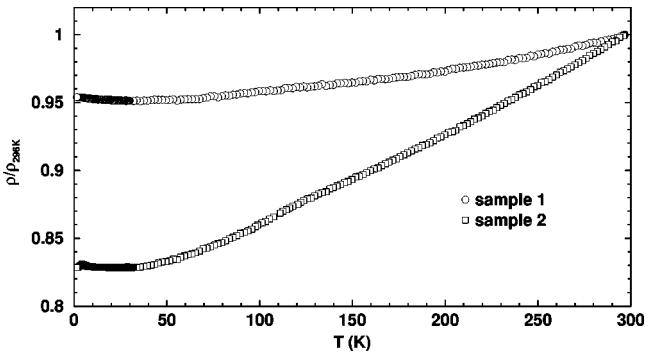

FIG. 8. Temperature dependence of the resistivity normalized to its values $\rho_{296\ K}=350\mu\Omega$ cm (sample 1) and $\rho_{296\ K}=199\mu\Omega$ cm (sample 2) at $T=296$ K in the temperature range 1.5 K$<T<$296 K.

TABLE I. Experimental results: specific heat (Sommerfeld constant γ) (column 2), Debye energy Θ_0 (column 3), residual resistivity ratio (RRR) (column 4), and resistivity $\rho_{296\ \mathrm{K}}$ at $T=296$ K.

Sample No.	γ [mJ/mol K^{-2}]	Θ_0 [K]	RRR	$\rho_{296\ \mathrm{K}}$ $\mu\Omega$ cm
1	2.8	415	1.05	350
2	2.0	419	1.2	199

superconductivity as was found from magnetization and resistance measurements.

Sizable deviations from the linear fits, shown in Fig. 6, are observed especially for sample No. 1 and to a minor degree but with the opposite curvature also for sample No. 2. Similar deviations as found for these two samples are known as well from MgB_2.[21–23] Since there such anomalous contributions do not essentially change in the superconducting state, we ascribe them to lattice effects related to boron disorder present in all diborides.

Naturally, the initial Debye temperature $\Theta_0 \approx 417 \pm 2$ K is smaller than the corresponding value reported for MgB_2 of 750–800 K.[24,22,21] But it is somewhat *harder* than the value one might expect from a simple scaling with the square root of the total mass ratio: 369 ± 11 K. This is in line with the hardening calculated for the optical phonons at the Γ point as reported above.

The theoretically estimated value of the el-ph coupling constant λ is in accordance with those small λ values derived by comparing the experimental value of the Sommerfeld constant (see Fig. 6) with the calculated DOS at the Fermi level $N(\varepsilon_F)$:

$$\gamma_{expt} = (\pi^2/3) k_B^2 (1+\lambda) N(\varepsilon_F) = \gamma_0 (1+\lambda). \qquad (3)$$

Using our calculated $\gamma_0 = 2.14$ mJ/mol K^2 and the measured $\gamma_{expt} = 2.8$ mJ/mol K^2 of sample No. 1, we obtain an empirical value of $\lambda_{\mathrm{No.\ 1}} = 0.3$. If this estimate is correct, a sizable contribution of relatively low-frequency phonons involving Ta vibrations can be expected (See Table I).

The low value of $\gamma_{expt} = 2$ mJ/mol K^2 for sample No. 2 can be ascribed to the significant number of boron vacancies in understoichiometric $TaB_{2-\delta}$ samples. Within a very crude estimate, supposing a rigid band behavior and using the atomic partial density of states $N_{Ta}(\varepsilon_F)$ and $N_B(\varepsilon_F)$ (see Fig. 1) we assume, for the effective bare specific heat constant $\gamma_{0,eff}$,

$$\gamma_{0,eff} < (\pi^2/3) k_B^2 [N_{Ta}(\varepsilon_F) + (2-\delta) N_B(\varepsilon_F)]. \qquad (4)$$

For $TaB_{1.29}$ (sample No. 2) this yields $\gamma_{0,eff} = 1.8986$, corresponding to $\lambda_{\mathrm{No.\ 2}} = 0.053$. Considering additionally broadening effects in the DOS due to disorder in the vacancy distribution and other impurities, which λ value can be taken as a lower bound.

Adopting a standard value of the Coulomb pseudopotential $\mu^* = 0.13$ one arrives at negligible values of the transition temperature $T_c \sim 10^{-7}$ K, irrespectively of the details of the shape of the Eliashberg function, i.e., the averaged phonon frequency. If even the pseudopotential μ^* were ignored, T_c would not exceed 18 mK. Thus, the experimental evidence for the absence of superconductivity, possibly even down to several 100 mK,[5] becomes very plausible already in the traditional electron-phonon Migdal-Eliashberg picture.

IV. CONCLUSIONS

Although TaB_2 occurs in the same crystal structure as MgB_2, it should not be considered as a close relative of MgB_2 with respect to the electronic structure (even if it would be found superconducting at very low temperatures). The major differences occur due to (i) the different band filling because of the three additional valence electrons of Ta with respect to Mg, resulting in a shift of the the Fermi level from the bonding B-σ states in MgB_2 to the antibonding B-σ–Ta-d hybrid states in TaB_2 , (ii) the strong out-of-plane hybridization of the B $2p$ states with Ta, and (iii) the weak electron-phonon coupling, especially of the E_{2g} mode, which is strongly coupled in MgB_2 . Furthermore, TaB_2 differs significantly from MgB_2 with respect to the coupling of the E_{2g} mode to various parts of the Fermi surface. In the latter, the σ-dervied tubes are most deformed, whereas in TaB_2 both large sheets (see Fig. 4) are involved. Hence, in MgB_2 a multiband description[25–27] is necessary, whereas in TaB_2 the situation is less clear. In some sense, such an attempt to divide the electrons at the Fermi surface with respect to superconductivity in various subgroups is even meaningless due to the generally weak electron-phonon interaction.

According to our experimental results, TaB_2 is not superconducting down to 1.5 K. Thus, we confirm the earlier results of Refs. 10 and 5 and disprove at the same time the speculation about superconductivity around 9.5 K reported in Ref. 8. Because in our opinion the main reason for the absence of superconductivity in TaB_2 is the different position of the Fermi level (with respect to MgB_2), huge hole doping might ''reintroduce'' superconductivity at relatively high temperatures.

In other words, the results obtained here suggest that the empirical absence or low-temperature superconductivity established in many transition metal (or rare earth) diborides with *electrons* as the potentially paired charge carriers, stressed by Hirsch,[28] might be explained in the traditional electron-phonon picture simply by a *weak* electron-phonon interaction. In that case there is no need to explain this behavior by the absence of a sophisticated Coulomb-interaction-driven nonphonon mechanism which works exclusively for holes.[28]

Corresponding studies for other related transition metal diborides of experimental interest will be published elsewhere.

ACKNOWLEDGMENTS

We thank J.M. An and S.V. Shulga for discussions and N. Mattern for providing us with the XRD data. This work was supported by the DAAD (individual grant to H.R.), ONR Grant No. N00017-97-1-0956, and the Deutsche Forschungsgemeinschaft, SFB 463.

*Corresponding author. Electronic address: helge@physics.ucdavis.edu

[1] J. Nagamatsu, N. Nakagawa, T. Muranaka, Y. Zenitani, and J. Akimitsu, Nature (London) **410**, 63 (2001).

[2] J.S. Slusky, N. Rogado, K.A. Regan, M.A. Hayward, P. Khalifah, T. He, K. Inumaru, S. Loureiro, M.K. Haas, H.W. Zandbergen, and R.J. Cava, Nature (London) **410**, 343 (2001).

[3] I. Felner, Physica C **353**, 11 (2001).

[4] Y.G. Zhao, X.P. Zhang, P.Y. Qiao, H.T. Zhang, S.L. Jia, B.S. Cao, M.H. Zhu, Z.H. Han, X.L. Wang, and B.L. Gu, cond-mat/0103077 (unpublished).

[5] G.V. Samsonov and I.M. Vinitsky, *Refractory Compounds* (Metallurgia, Moskva, 1976).

[6] A.S. Cooper, E. Corenzerst, L.D. Longinotti, B.T. Mattias, and W.H. Zachariasen, Proc. Natl. Acad. Sci. U.S.A. **67**, 313 (1970).

[7] L. Leyarovska and E. Leyarovski, J. Less-Common Met. **67**, 249 (1979).

[8] D. Kaczorowski, A.J. Zaleski, O.J. Zogal, and J. Klamut, cond-mat/0103571 (unpublished).

[9] D. Kaczorowski, J. Klamut, and A.J. Zaleski, cond-mat/0104479 (unpublished).

[10] V.A. Gasparov, N.S. Sidorov, I.I. Zver'kova, and M.P. Kulakov, cond-mat/0104323 (unpublished).

[11] K. Koepernik and H. Eschrig, Phys. Rev. B **59**, 1743 (1999).

[12] J.P. Perdew and A. Zunger, Phys. Rev. B **23**, 5048 (1981).

[13] H. Eschrig, *Optimized LCAO Method and the Electronic Structure of Extended Systems* (Springer, Berlin, 1989).

[14] P.P. Singh, cond-mat/0104580 (unpublished).

[15] Our band structure calculations for MgB_2 are in excellent agreement with those of Refs. 16 and 17. The partial DOS naturally differ from Ref. 17 because of different calculational methods. To calculate the partial DOS, we use the projection onto our minimal basis set instead of a projection onto muffin tin spheres in Ref. 17, which finds a large contribution of the interstitial plane-wave region.

[16] J.M. An and W.E. Pickett, Phys. Rev. Lett. **86**, 4366 (2001).

[17] J. Kortus, I. I. Mazin, K. D. Belashchenko, V. P. Antropov, and L. L. Boyer, Phys. Rev. Lett. **86**, 4656 (2001).

[18] The published lattice constants for TaB_2 scatter much stronger than the usual experimental errors in an XRD experiment. We found parameter sets reported with 3.057 Å$<a<$3.0966 Å and 3.224 Å$<c<$3.288. (Refs. 10, 29, and 30). The different lattice constants are most probably due to different B contents of different samples.

[19] K.-P. Bohnen, R. Heid, and B. Renker, Phys. Rev. Lett. **86**, 5771 (2001).

[20] F.S. Kahn and P.B. Allen, Phys. Rev. B **29**, 3341 (1984).

[21] Y.X. Wang, T. Plackowski, and A. Junod, Physica C **355**, 179 (2001).

[22] R.K. Kremer, B.J. Gibson, and K. Ahn, cond-mat/0102432 (unpublished).

[23] E. Bauer, Ch. Paul, St. Berger, S. Majumdar, H. Michor, M. Giovannini, A. Saccone, and A. Bianconi, J. Phys.: Condens. Matter **13**, L487 (2001).

[24] S.L. Bud'ko *et al.*, Phys. Rev. Lett. **86**, 1877 (2001).

[25] S.V. Shulga, S.-L. Drechsler, H. Eschrig, H. Rosner, and W.E. Pickett, cond-mat/0103154 (unpublished).

[26] H. Rosner, J.M. An, W. Ku, M.D. Johannes, R.T. Scalettar, W.E. Pickett, S.V. Shulga, S.-L. Drechsler, H. Eschrig, W. Weber, and A.G. Equiluz, in *Studies of High Temperature Superconductors*, edited by A.V. Narlikar (Nova Science, NY, 2001), Vol. 38.

[27] G. Fuchs, S.-L. Drechsler, S.V. Shulga, K.-H. Müller, A. Handstein, K. Nenkov, and H. Rosner, in *Studies of High Temperature Superconductors*, edited by A.V. Narlikar (Nova Science, NY, in press), Vol. 39.

[28] J.E. Hirsch, Phys. Lett. A **282**, 392 (2001).

[29] P. Villars and L.D. Calvert, *Pearson's Handbook of Crystallographic Data for Intermetallic Phases* (Materials Information Society, Materials Park, OH, 1991), Vol. 2, pp. 16 939–16 940.

[30] S. Otani, M.M. Korsukova, and T. Mitsuhashi, J. Cryst. Growth **194**, 430 (1998).